

Influence of axial load on behavior of belled pile reinforced with high-strength steel bars



Y. Hibino

Tokyo Institute of Technology, Japan

S. Suzuki

Kajima Corporation, Japan

Y. Shinohara

Tokyo Institute of Technology, Japan

S. Hayashi

Tokyo Institute of Technology, Japan

SUMMARY:

The influence of axial load on flexural behavior of the concrete belled piles reinforced with high-strength steel bars was drawn from the experimental test result: 1) the absence of axial load causes fracture of the longitudinal reinforcements on the tensile side; 2) the reinforcement experienced buckling and fracture under high axial load; 3) the domination of a rotation at hinge region was enhanced by higher axial load ratio and decreased cracks distribution; 4) the effective stiffness can be estimated by the existing formula, though estimations gives a small overestimation in high axial load ratio.

Keywords: Piles, Flexural behavior, High-strength steel bars, Axial load

1. INTRODUCTION

Belled piles have been used for mid- or high-rise reinforced concrete buildings in expectation of its high-axial load capacity. The concrete pile is primary compression members of building, and piles are subjected to axial compression and tension stresses caused by bending during earthquakes. Structural design of piles provided by ACI 543R-00 (2000) were developed using strength design principle from ACI 318-95 (1995), and the design strength of the pile subjected to flexure combined with axial compression computed by multiplying the nominal strength of the pile by a strength reduction factor, which piles is treated as columns in accordance with ACI 318-95 (1995).

Recently, through the growing use of performance based design, the ultimate strength calculation of the piles is considered to ensure the sufficient seismic capacity of buildings in term of strength, ductility, and durability. On the other hand, reinforcement congestion and poor concrete placement are common issues found in belled pile using conventional steel bars. The use of high-strength steel as longitudinal or transverse reinforcement is one solution to solve the issue. Nagae et al. (2000) studied the pile reinforced with high-strength transverse reinforcement, and reported that increasing of shear strength, and the pile had large flexural capacity. Hibino et al. (2011) conducted experimental tests of belled pile reinforced with high-strength steel bars under a constant axial compression, and evaluated the belled pile reinforced with high-strength steel bars has equivalent flexural ductility to existing piles under an axial load. However, the piles can experience repeated tension and compression axial load under seismic excitation; hence more investigation of flexural behavior of the belled pile under various axial loads is required.

To investigate effect of axial compression load on flexural behavior, this paper presents experimental tests on belled piles reinforced with high-strength steel bars subjected to flexural behavior. These tests provided the flexural behavior under combined various axial and flexural loading, and assessment of those effective stiffness.

2. EXPERIMENTAL TEST PROGRAM

2.1. Test specimens

A summary of the main properties of the specimens is shown in Table 2.1. There are two series specimens with different concrete strength. Geometric properties of the specimens are shown in Figure 2.1. The specimens were fabricated as 1/5-scale pile assuming application in mid-story reinforced concrete building, and twenty D10 high strength longitudinal reinforcements and 5.1 mm diameter of high strength spiral web reinforcements with 50 mm pitch spacing were used. The constant axial compression load: 407.4 kN; 814.8 kN; 1222.2 kN, were applied to the specimen, which loads were determined by assuming suffered axial load of piles at a corner end during earthquake. The shear span-to-depth ratio, $M/VD=2.5$ is constant for all the specimens, which was assumed by Chang's method (Chang 1937). Compressive strengths of concrete were targeted as 24 MPa for L series specimen and 36 MPa for M series specimen. Material properties of steel are shown in Table 2.2. Elongation ratio of the steels of D10 and U5.1 has about 7 % which is lower than that of conventional steels.

Table 2.1. Properties of test specimens

Specimen		Longitudinal reinforcement		Transverse reinforcement		P kN	f'_c , MPa	E_c , MPa	σ_0/f'_c
		Reinforcing bar	ρ_{st} , %	Reinforcing bar	ρ_t , %				
L	LN	20-D10 (SPR785)	1.5	U5.1@50 mm (SBPD1275)	0.26	0	23.1	27400	0
	LL					407.4			0.17
	LS					814.8			0.34
	LU					1222.2			0.51
M	MN	20-D10 (SPR785)	1.5	U5.1@50 mm (SBPD1275)	0.26	0	36	32400	0
	ML					407.4			0.12
	MS					814.8			0.24

Note: D is pile diameter, ρ_{st} is ratio of total area of longitudinal reinforcement to gross concrete area, ρ_t is ratio of area distributed transverse reinforcement to gross concrete area perpendicular to that reinforcement, P is axial load, f'_c is concrete compressive strength, E_c is young's modulus of concrete, and σ_0 is effective stress on cross section.

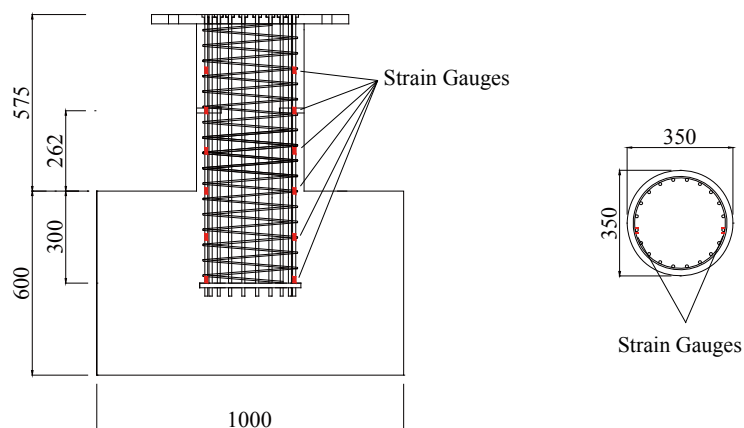


Figure 2.1. Geometric properties of test specimen (unit: mm)

Table 2.2. Steel characteristic

Steel type	f_y , MPa	f_{su} , MPa	E_s , MPa
D10	885	931	194000
U5.1	1378	1448	174000

Note: f_y is yield strength of steel, f_{su} is ultimate steel strength, and E_s is young's modulus of steel.

2.2. Test setup

Bi-directional cyclic loading tests were conducted using the test rig shown in Figure 2.2. The cyclic lateral load applied by cantilever system with horizontal jack who are installed in the bottom of the frame. Vertical jacks who have two pin hinges at both ends are installed in the top of the frame to apply a constant axial load at the top of the pile. The reaction block installed on top of specimen can be rotated in accordance with the deflection and rotation of the pile, and connects specimen and vertical jacks rigidly. A slider is placed between a reaction block and the frame to free horizontal movement of the pile during lateral cycling loading while maintaining the vertical load. Loading directions are shown in shown in Figure 2.2 beside arrow symbol. The tests were controlled by deflection angle, R obtained from the horizontal displacement divided by shear span length (875 mm). The loading history was as follows: $R=\pm 1/400 \times 1$, $R=\pm 1/200 \times 2$, $R=\pm 1/100 \times 2$, $R=\pm 1/67 \times 2$, $R=\pm 1/50 \times 2$, $R=\pm 1/33 \times 2$, and $R=\pm 1/25 \times 1$. After the last loading cycle, the positive direction monotonic load applied to the specimen MS until a fracture of longitudinal reinforcement.

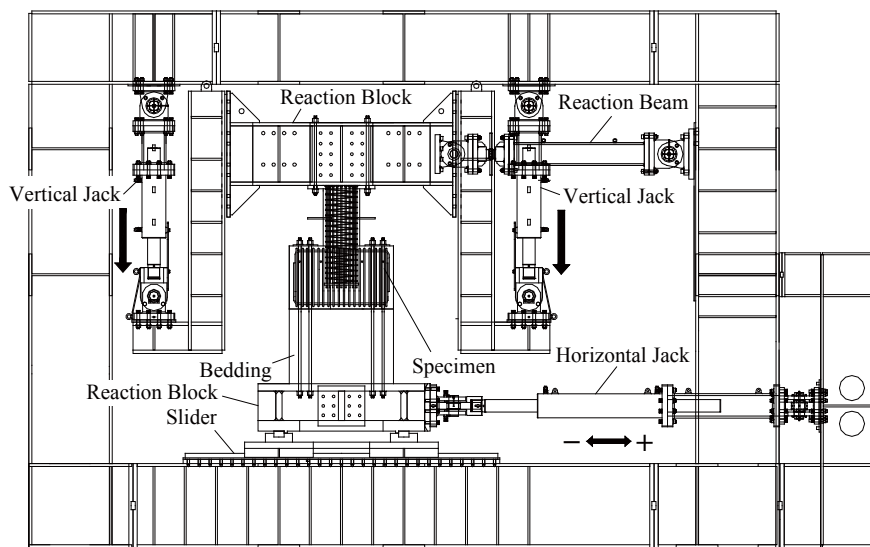


Figure 2.2. Test setup

2.3. Test results

Observed crack drawings and picture are shown in Figure 2.3. The drawings are drawn for development elevation, and the solid and broken lines represent cracks occurred during positive and negative loading, respectively. First bending cracks were observed at the pile fixed end, afterward the cracks were spread upward with an increasing of shear force, and then shear cracks increased with an increasing of deformation. The shear cracks of the specimen LN spread finer than that of the other specimens, whereas number of cracks of the specimen LU is small and concrete crushing occurs. This indicates that the rotation of the hinge region dominated in deflection which is enhanced by concrete crushing due to high axial load.

Comparisons between the measured lateral load versus deflection are shown in Figure 2.4. Broken line represents predictions listed in Table 2.3 obtained by fiber section analysis considering $P-\delta$ effect. Square, circle, triangle and diamond symbols are drawn at the points where concrete crushing at the fixed end, flexural yielding of longitudinal reinforcements, peak shear strength and fracture of reinforcements, respectively. The observed and predicted shear strength in failure after flexural yielding and fracture mode for the piles are summarized in Table 2.3. The cyclic loading of all the specimens shows that large flexural ductility after deflection of 0.02 rad in compared with the pile having conventional steel bars; however, small strength degradation is observed after fracture of reinforcement for the specimen LN, LS, MN and MS. The fracture of main steel bars observed in the specimen LN and MN, and buckling before fracture was observed in the specimen LS and MS. Hence,

the buckling affected fracture of reinforcement, and the fracture is due to lower elongation, compared with conventional steels, of high-strength steel bars. The flexural yielding of the specimens occurred at $R=1/100$ after compression failure of concrete due to the high axial load in the specimen LN and LU, whereas the flexural yielding occurred prior to concrete crushing in the other specimens. The predictions of the specimen are almost agreed with the peak shear strength, V_{max} , and the peak shear strength was increased with an increasing of the axial load.

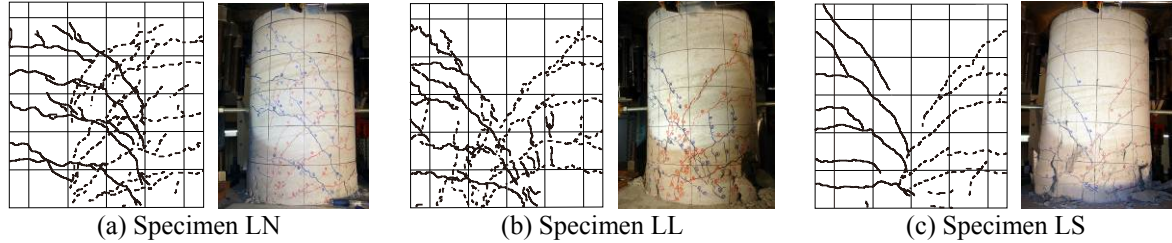


Figure 2.3. Crack patterns of the piles after failure

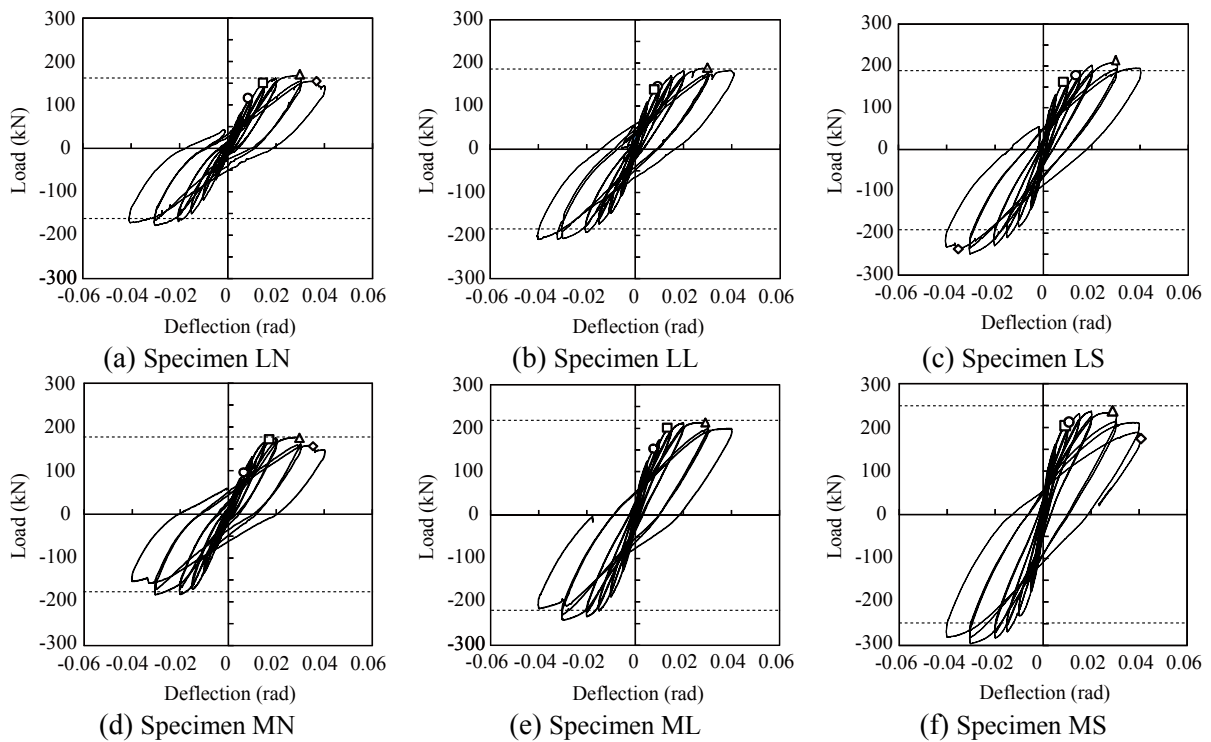


Figure 2.4. Experimental lateral load-displacement relationship

Table 2.3. Summary of test results

Specimen	V_p , kN	V_{max} , kN		V_{max}/V_p	Fracture mode	EI_e , kN/mm	EI_g , kN/mm	$EI_{g,calc.}$, kN/mm	EI_e/EI_g	$EI_e/EI_{g,calc.}$
		Positive direction	Negative direction							
LN	162	168	-177	1.09	Tension	12.3	34.5	91.8	0.36	0.13
LL	190	188	-209	1.13	-	16.9	70.9	91.8	0.24	0.18
LS	199	209	-249	1.31	Buckling	19.2	131.4	91.8	0.15	0.21
LU	186	212	-272	1.55	Buckling	19.7	55.6	91.8	0.36	0.21
MN	179	177	-184	1.03	Tension	15.4	48.3	106.4	0.32	0.14
ML	224	213	-242	1.11	-	17.3	80.8	106.4	0.21	0.16
MS	254	237	-296	1.19	Buckling	21.3	176.2	106.4	0.11	0.18

Note: V_p is prediction, V_{max} is peak strength and fracture mode is tension (Tension) or tension after buckling (Buckling), and EI_e is effective stiffness, EI_g is gross-section stiffness, and $EI_{g,calc.}$ is calculated gross-section stiffness ($=a^3/3E_cI+\kappa a/GA_g$)⁻¹. Where I is moment of inertia of section about centroidal axis, κ is shape index, G

is modulus of transverse elasticity, and A_g is gross cross-sectional area.

The effective stiffness, EI_e and gross-section stiffness, EI_g obtained by experimental results, which is defined by a diagonal line connecting between origin and the first point at which the tension reinforcement yielded or concrete crushing occurred, whichever came first on force-displacement envelope as shown in Figure 2.5. The effective stiffness is increased by increasing of concrete strength. But, the experimental gross-section stiffness is not agreed with calculated one because of crack or loading condition. Figure 2.6 shows relationship between effective stiffness ratio EI_e/EI_g and axial load ratio. The solid and blank symbols represent effective stiffness ratio calculated by experimental effective stiffness and calculated effective stiffness, respectively, using calculated gross-section stiffness. The calculated stiffness was obtained by fiber section analysis assuming the hinge height of $0.75D$ (262 mm). Solid and chain line represents following effective stiffness ratio proposed by Elwood et al. (2009) with two options for d_b/D .

$$\frac{EI_e}{EI_g} = \frac{0.45 + 2.5P/A_g f'_c}{1 + 110 \left(\frac{d_b}{D}\right) \left(\frac{D}{a}\right)} \leq 1.0 \text{ and } \geq 0.2 \quad (2.1)$$

where d_b is nominal diameter of longitudinal bars, and the d_b/D can be approximated as 1/24 for bridge columns and 1/18 for building columns. The trends of analysis results are agreed with experimental results. The stiffness increases with an increasing of axial load ratio. Estimation by Elwood and similarly increase with an increasing of axial load ratio; however, the estimation overestimates the stiffness especially with high axial load.

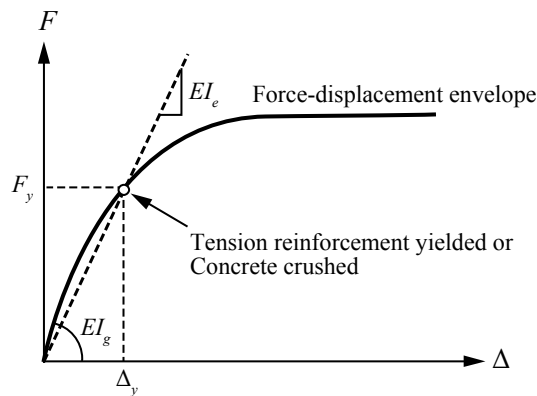


Figure 2.5. Definition of effective stiffness

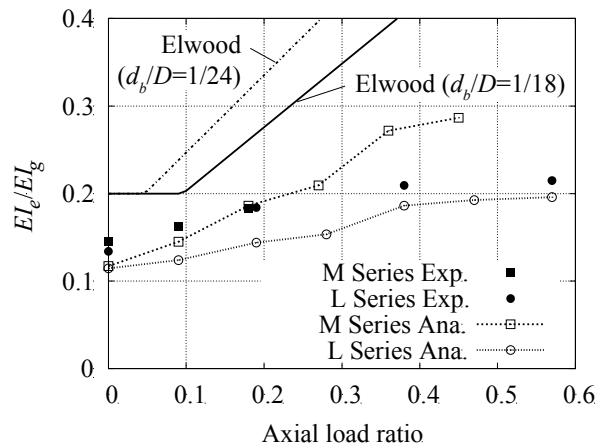


Figure 2.6. Relationship between effective stiffness and axial load ratio

2.4. Strains on longitudinal reinforcements

Measured peak strain of reinforcement at loading cycles of $R=1/400$, $R=1/200$, $R=1/100$, $R=1/67$ and $R=1/33$ are shown in Figure 2.7. The strain data is measured by strain gauges installed on longitudinal reinforcements arranged at tensile and compressive side. The vertical axis represents the position of the strain from the pile fixed end, which is illustrated in Figure 2.1 with red square symbols, and dashed line represents yielding strain. The positive and negative values of strain mean tensile and compressive strain, respectively. The tensile strain at the fixed end of the specimen MN yielded at the cycle of $R=1/67$, and after the cycle the strain increased more than 20000μ . On the other hand, for the specimen MS the strain yielded at $R=1/67$, and the strain of compressive side reinforcement exceeded 15000μ at the cycle of $R=1/33$ where the height of 130 mm, which indicates that the steel experienced buckling by high axial load.

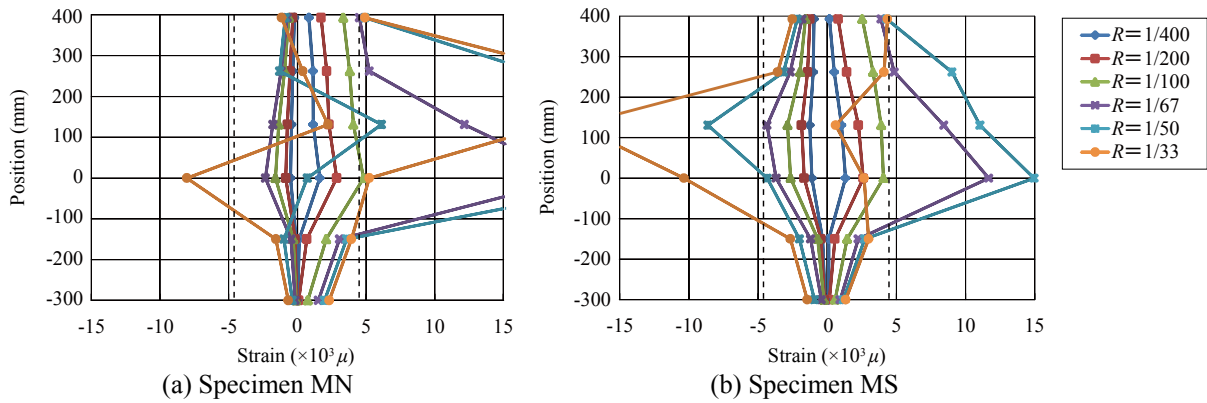


Figure 2.7. Peak strain of reinforcement

Figure 2.8 shows fractured reinforcement taken from specimens MN and LS by drilling after the experimental test. The fracture surface is different between the specimens: the steel of the specimen MN is constricted in the middle; and the steel of the specimen LS has sharply cut surface. The buckling occurred at the second spacing of the hoop from the fixed end which height is about 130 mm (see Figure 2.8(c)) as same as the position of the peak strain data at $R=1/33$ shown in Figure 2.7(b).



Figure 2.8. Fractured reinforcements

2.5. Contribution of components to total displacement

Total displacement of the pile, Δ_H can be defined as follows.

$$\Delta_H = \Delta_{H,pile} + \Delta_{H,hinge} \quad (2.2)$$

where $\Delta_{H,pile}$ is deformation of a part of the pile except hinge region (see Figure 2.9) attributable to flexure, and $\Delta_{H,hinge}$ is the hinge deformation. The hinge region was defined as $0.75D$ height from the fixed end. Additionally, total displacement Δ_H is calculated as follows.

$$\Delta_H = \Delta_{H,pile,T} + \frac{l_{frame} (\Delta_{V,pile,R} + \Delta_{V,pile,L})}{L_{pile}} \quad (2.3)$$

where $\Delta_{H,pile,T}$ is deformation at the top of the specimen, l_{frame} is distance from the loading height to the top of the specimen, $\Delta_{V,pile,L}$ and $\Delta_{V,pile,R}$ are vertical deformation caused by rotation of the specimen, and L_{pile} is span between the measurement points of $\Delta_{V,pile,L}$ and $\Delta_{V,pile,R}$. Hence, the hinge deformation attributable to flexure, $\Delta_{H,hinge}$ is derived as follows assuming the pile has a linear variation in curvature over the height of the hinge.

$$\Delta_{H,hinge} = \theta_{hinge} (a - l_{hinge}) = \frac{\Delta_{V,hinge,R} - \Delta_{V,hinge,L}}{L_{hinge}} (a - l_{hinge}) \quad (2.4)$$

where θ_{hinge} is rotation caused by the deformation of the hinge region, $\Delta_{V,hinge,L}$ and $\Delta_{V,hinge,R}$ are vertical deformation, and L_{hinge} is span between the measurement points of $\Delta_{V,hinge,L}$ and $\Delta_{V,hinge,R}$, a is shear span (875 mm), and l_{hinge} is height of hinge region ($0.75D$). The lateral displacement of the pile due to slip of the reinforcing bar is given by following equation integrating the triangular strain diagram using measured strain as shown in Figure 2.9.

$$\Delta_{H,slip} = \theta_{slip} a = \frac{\int \varepsilon_s}{\{c - (d_t + j)\}} a \quad (2.5)$$

where θ_{slip} is rotation at the end of the pile, ε_s is strain of reinforcing bar in footing, c is neutral axis calculated by $\Delta_{V,hinge,L}$ and $\Delta_{V,hinge,R}$ assuming Navier's hypothesis on assumption that which is the same at the fixed end, d_t is distance between tensile end and rebar's position, and j is distance from the measurement position of $\Delta_{V,hinge,R}$ to pile end. Note that the deformation, Δ_{slip} is considered till before a cycle when reinforcement yielded and after the cycle the displacement was assumed as constant. The lateral displacement of the hinge region due to in flexure, $\Delta_{H,hinge,flex}$ is given by following expression. If the deformation, $\Delta_{H,slip}$ is larger than the deformation, $\Delta_{H,hinge}$, the deformation, $\Delta_{H,hinge,flex}$ is assumed to be zero.

$$\Delta_{H,hinge,flex} = \Delta_{H,hinge} - \Delta_{H,slip} \quad (2.6)$$

The deformation attributable to a part of the pile except hinge region, $\Delta_{H,pile}$ is obtained by Eq. (2.2) assuming that slip of reinforcing bar in a part of the pile except hinge region is not cause.

Figure 2.10 shows contribution of components to total displacement on the peak of each loading cycle. The total displacement on each loading cycle represents target displacement of the cycle. The deformation, $\Delta_{H,pile}$ is almost constant after the cycle of 1/100 when the longitudinal reinforcement yielded in all the specimens, consequently the deformation, $\Delta_{H,slip}$ is constant, and the deformation of the hinge region, $\Delta_{H,hinge,flex}$ dominated after yielding. The deformation, $\Delta_{H,slip}$ of the specimen LN at the cycle of 1/100 is larger than that of the specimen LU due to the absence of axial load, and the deformation, $\Delta_{H,hinge,flex}$ of the specimen LU is larger than the that of the specimen LS because of the concrete crushing in hinge region due to high axial load. This indicates that hinge rotation was enhanced by higher axial load ratio, and decreased cracks distribution.

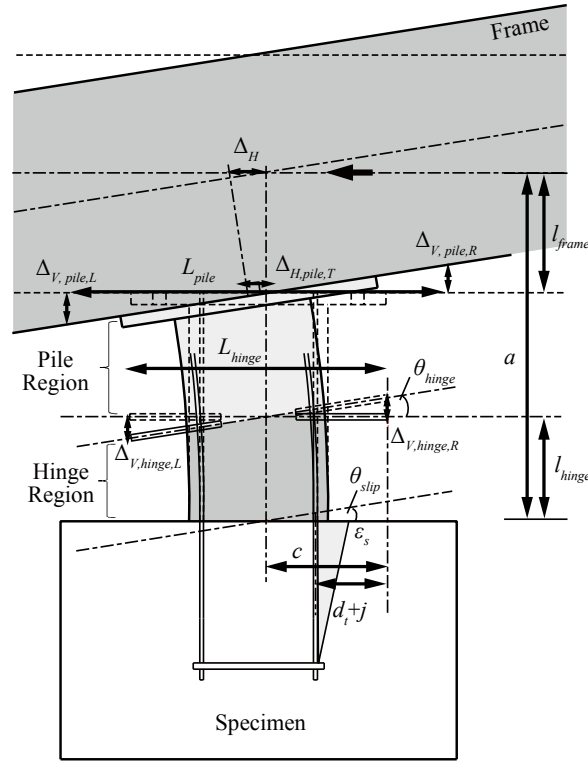


Figure 2.9. Definition of deformations

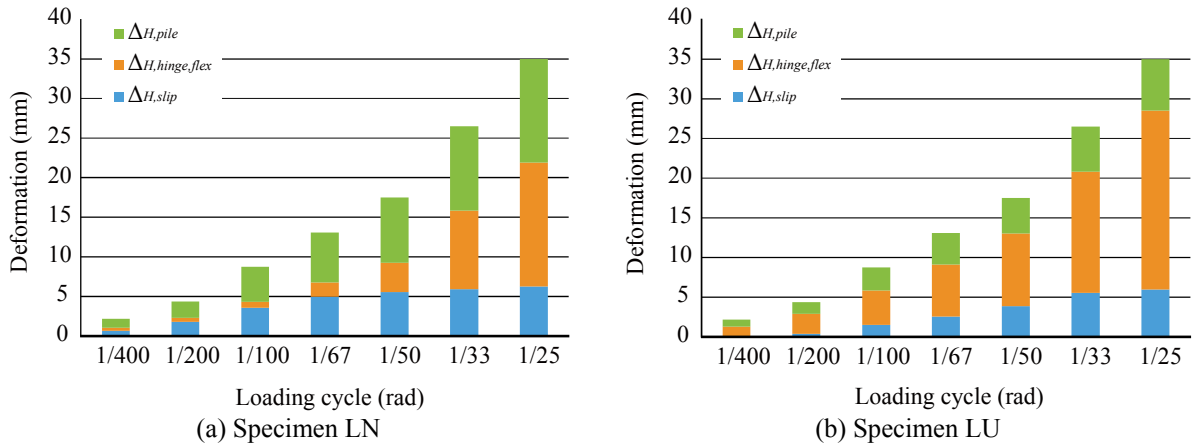


Figure 2.10. Contribution of components to total displacement

3. ASSESMENT OF EFFECTIVE STIFFENSS

Architectural Institute of Japan (AIJ) (1999) provides the ratio of effective stiffness for rectangular column as follows.

$$\frac{EI_e}{EI_g} = \left(0.043 + 1.64n\rho + 0.043 \frac{a}{D_c} + 0.33 \frac{\sigma_0}{f'_c} \right) \left(\frac{d}{D_c} \right)^2 \quad (3.1)$$

where n is modular ratio (E_s/E_c), ρ is ratio of tension reinforcement to gross sectional area, $\rho = \rho_{st}/4$, D_c is column height, and d is distance from tension reinforcement to compression side. To apply the effective stiffness for circular column, equivalent height, $D_e = D/2\sqrt{\pi}$, can be substituted for column height, D_c . Figure 3.1 shows comparison of estimated effective stiffness and experimental test. The

estimation by Elwood overestimates the stiffness for specimens with high axial load as shown in Figure 2.6; however, the estimation by AIJ shows good agreement with experimental results except the specimen LU. AIJ formula can estimate the effective stiffness ratio regardless of axial load ratio, though both estimations overestimate in high axial load.

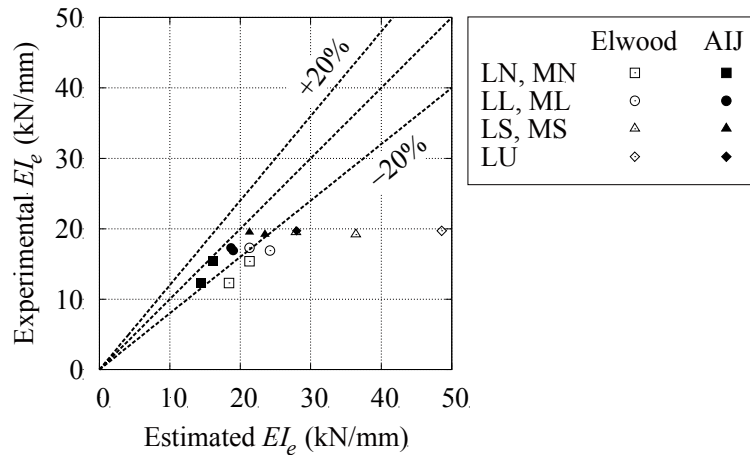


Figure 3.1. Comparison of estimated and experimental effective stiffness

4. CONCLUSIONS

This paper presents the experimental result aiming to study the behavior and ductility of belled pile reinforced with high-strength steel bars under cyclic loading. The influence of axial load on flexural behavior of the belled piles reinforced with high-strength steel bars was drawn from the experimental test result as shown in followings.

The ultimate strength of the piles with high-strength steel bars can be designed using cross-sectional analysis. All test piles reinforced with high-strength reinforcement have a sufficient flexural ductility in compared with the pile having conventional steel bars. The absence of axial load causes fracture of the longitudinal reinforcements on the tensile side. This fracture is due to lower elongation, compared with conventional steels, of high-strength steel bars after yielding.

The high-strength longitudinal reinforcement of the piles experienced buckling and fracture under high axial load, when strength degradation occurred in the hysteresis. The domination of a rotation at hinge region was enhanced by higher axial load ratio, and decreased cracks distribution.

The effective stiffness can be estimated by the existing formula considering equivalent rectangular cross-sectional area to circular area, though the estimations of the specimen with high axial load ratio give a small overestimation.

AKNOWLEDGEMENT

The authors wish to acknowledgement the supplier of the reinforcement; Neturen Co., Ltd., and Tokyo Tekko Co., Ltd.

REFERENCES

- American Concrete Institute. (1995). Building Code Requirements for Structural Concrete (ACI 318-95) and Commentary, American Concrete Institute, Michigan, USA.
- American Concrete Institute. (2000). Design, Manufacture, and Installation of Concrete Piles (ACI 543R-00), American Concrete Institute, Michigan, USA.
- Architectural Institute of Japan. (1999). Standard for Structural Calculation of Reinforced Concrete Structures –Based on Allowable Stress Concept–, Architectural Institute of Japan, Tokyo, Japan. (in Japanese)

- Chang, Y. L. (1937). Discussion on "Lateral Pile-Loading Tests" by LB Feagin. *Transaction of ASCE*. **102**, 272-278.
- Elwood, K. J., Eberhard, M. O. (2009). Effective stiffness of reinforced concrete column. *ACI structural journal*. **106:4**, 476-484.
- Hibino, Y., Shinohara, Y., and Hayashi, S. (2011). Flexural behavior of belled pile with high-strength longitudinal reinforcement. *8th International Conference on Urban Earthquake Engineering*. 819-824.
- Nagae, T., Wang, J., Katori, K., and Hayashi, S. (2000). Shear crack and failure process of slip reinforced concrete pile. *Concrete Journal*. **22:3**, 619-624. (in Japanese)